CMM 2022 & 42nd SolMech 2022

Granular computational homogenisation of composite structures with imprecise parameters

W. BELUCH[1)], M. HATŁAS[2)], J. PTASZNY[1)]

[1)] *Silesian University of Technology, Department of Computational Mechanics and Engineering, Konarskiego 18A, 44-100 Gliwice, Poland, e-mail: witold.beluch@polsl.pl*

[2)] *Silesian University of Technology, Konarskiego 18A, 44-100 Gliwice, Poland*

THE PAPER PRESENTS THE FORMULATION OF A GRANULAR COMPUTATIONAL HO-MOGENISATION PROBLEM and the proposition of a method to solve it, which enables multiscale analysis of materials with uncertain microstructure parameters. The material parameters and the geometry, represented by the interval and fuzzy numbers, are assumed to be unprecise. An α-cut representation of fuzzy numbers allows the use of interval arithmetic for epistemic uncertainties. Directed interval arithmetic is used to reduce the effect of interval widening during arithmetic operations. Response surfaces of diverse types, including Artificial Neural Networks, are used as model reduction methods. The finite element method is employed to solve the boundary value problem on a micro scale. Numerical examples are provided to demonstrate the effectiveness of the proposed approach.

Key words: computational homogenisation, granular computations, fuzzy numbers, directed interval arithmetic, response surfaces, finite element method.

1. Introduction

INHOMOGENEOUS MATERIALS, SUCH AS COMPOSITES OR POROUS MATERIALS, are becoming an increasingly important group in modern engineering because they may possess properties that are unavailable to homogeneous structural materials. As a result, they are widely used in many industries such as mechanical, automotive, marine, aerospace, etc. The macroscopic mechanical properties of inhomogeneous materials are strongly determined by their microscopic structure [1]. The development of composite manufacturing technology allows the creation of composites with specific macroscopic properties [2]. Disregarding phenomena occurring at lower scales may result in creating models that do not adequately reflect the behaviour of real materials. This requires the creation of a model which takes into account the different scales of the material – from the macro scale, where elements such as various external loads (mechanical, thermal, electrical, etc.) are taken into account, through the micro scale, taking into account e.g. discontinuities and surface imperfections (e.g. cracks, inclusions,

voids) to the nano scale, where e.g. defects in the crystal lattice can be taken into account. The relationship between the behaviour of the model at different scales is determined by the physical laws that correspond to each scale. The micro and macro scales are usually connected by the stress/strain state at each point in the material structure described by the constitutive law of the material.

The direct application of more than one scale in numerical calculations using one of the computational methods, such as the finite element method (FEM) or the boundary element method (BEM), leads to systems of equations with such a large number of degrees of freedom that a solution is usually not achievable with current computational capabilities. Homogenisation methods allow obtaining a macroscopically homogeneous medium equivalent to a microscopically heterogeneous one [3–5].

Typically, deterministic values of the input properties are assumed in the homogenisation procedure. However, due to manufacturing processes and measurement errors, it should be assumed that the properties of composite components are uncertain [6]. In this case, the macroscopic parametric values calculated using homogenisation methods are also uncertain.

Uncertain multiscale problems are considered by many authors. For example, a stochastic strategy and its implementation in a form of the Stochastic Finite Element Method for computational homogenisation of two-component particulate and fibrous composites with non-Gaussian random material characteristics is presented in [7]. In [8], a computational framework that combines the design of the experiment, computational homogenisation, and machine learning for data-driven analysis of composite materials under uncertainty is proposed. A sampling method that allows modelling non-stationary and spatial variations of uncertainty sources by creating nested random fields is proposed and applied in [9] for woven fibre composites.

According to [10], there exist three types of uncertainty: stochastic, informal (epistemic), and lexical. Uncertainty analysis methods are typically based on probabilistic analysis with stochastic input parameters, which allows consideration of linear and non-linear structures [11, 12]. To determine the statistical distribution of the input properties, a large number of experiments and measurements must be performed, which is usually time-consuming. For composite structures made in small series or individually, this information may not be available. In this case, a fuzzy or interval-based approach can be used to take into account the effects of epistemic uncertainty [13].

The direct use of fuzzy and interval calculations to solve boundary value problems and related linear systems of equations would result in a widening of output quantities, which is particularly inconvenient for complex numerical models [14]. Therefore, it may be beneficial to replace the full model with a metamodel that additionally may reduce the computational effort [15, 16].

An interval representation of fuzzy sets by α-cuts allows one to use interval arithmetic both for interval and fuzzy representation of uncertainties. There exist a few modifications of classic interval arithmetic that provide narrower final intervals, such as generalised interval arithmetic [17], segment analysis [18] or directed interval arithmetic [19]. The directed interval arithmetic can be considered a versatile and efficient technique.

The paper presents the formulation of a novel Granular Computational Homogenisation (GCH) problem and proposes an approach to its solution. Selected properties of the microstructure, i.e. geometry or constituent material parameters, are assumed to be imprecise and described using fuzzy numbers. The representation of the numbers involves α-cuts and directed interval arithmetic. Homogenisation requires the solution of boundary-value problems on the microscale, i.e. analysis of representative volume elements (RVEs) using FEM. As interval arithmetic uses the homogenisation results and requires many FEM simulations, the presented approach replaces the analyses with metamodels: response surfaces (RS) or neural networks. An application of metamodeling allows one to significantly reduce computational effort. The metamodeling process is preceded by the appropriate design of experiment, covering the domain of uncertain microstructure parameters. The minimised number of time-consuming FEM analyses makes the process robust. As a result of the whole GCH process, one obtains imprecise effective material constants represented by fuzzy numbers. One can use these imprecise constants to the uncertain description of a model of the structure on the macro scale.

The structure of the paper reflects the particular stages of the GCH solution process described in the above paragraph and is composed as follows. Section 2 introduces the concept of computational homogenisation. Section 3 describes granular calculations involving fuzzy numbers, interval numbers and directed interval arithmetic. Section 4 is devoted to model order reduction methods in the form of RS. The proposed Granular Computational Homogenisation approach is described in Section 5. Numerical examples that demonstrate the effectiveness of the proposed approach are collected in Section 6. The paper ends with conclusions (Section 7).

2. Computational homogenisation

Homogenisation is a part of multiscale modelling that allows one to model a structure at different length scales. This approach allows the analysis of materials that are inhomogeneous on the microscale, such as fibre-reinforced composites [20], particle-reinforced composites [21] or porous structures [22]. Multiscale problems concern the evaluation [23], identification [24], and optimisation [25] of material behaviour.

The use of homogenisation methods, which are part of multiscale calculations, allows one to obtain a macroscopically equivalent material model to a given inhomogeneous material by representing the macroscopic quantities of this material with variables that describe the state of the microstructure and its parameters [26]. Analytical homogenisation methods, such as asymptotic homogenisation [27], fast Fourier transform homogenisation [28] or semi-analytical mean-field homogenisation [29], have low computational requirements, but can only be used for simplified microstructure geometries and simple material models.

Unlike analytical and semi-analytical homogenisation methods, computational homogenisation can be applied effectively to the analysis of complex structures having linear and non-linear constitutive relationships [30]. According to [31], different variants of computational homogenisation allow considering different non-linearities, including path- and time-dependent models. Computational homogenisation uses numerical methods such as FEM or BEM to solve boundary value problems (BVPs) that describe the behaviour of a material at particular scales.

Computational homogenisation typically uses the representative volume element (RVE) concept. The RVE should represent the structure of the entire medium (or part of it in the case of local periodicity) and therefore contain all the information required to fully describe both the structure and properties of that medium [32]. The dimensions of the RVE are noticeably larger than the characteristic microscale dimensions and significantly smaller than the macroscale dimensions [33]. Moreover, the following conditions must be satisfied:

- The Hill–Mandel condition for the equality of microscopic mean energy density and macroscopic energy density at the point in the macrostructure corresponding to the location of the RVE:

$$(2.1) \qquad \langle \sigma_{ij} \varepsilon_{ij} \rangle = \langle \sigma_{ij} \rangle \langle \varepsilon_{ij} \rangle,$$

  where σ_{ij}, ε_{ij} are micro stress and strain tensors, respectively, $\langle \cdot \rangle$ is the averaged value of the field under consideration:

$$(2.2) \qquad \langle \cdot \rangle = \frac{1}{|V|} \int\limits_{V} (\cdot)\, dV,$$

  where V is the RVE domain.

- One of the prescribed boundary conditions satisfying the Hill–Mandel condition, e.g. in the form of:

  (i) periodic boundary conditions:

$$(2.3) \quad u_i^+ - u_i^- = \langle \varepsilon_{ij} \rangle \cdot (x_i^+ - x_i^-), \quad t_i^+ = -t_i^-, \ \forall x \in \Gamma : n_i^+ = -n_i^-,$$

where u_i^+, u_i^- are displacements of the corresponding points at the opposite RVE boundaries, x_i^+, x_i^- represent locations of the corresponding points at the opposite RVE boundaries, t_i^+, t_i^- are tractions on the corresponding points at the opposite RVE boundaries, n_i^+, n_i^- denote normal vectors at the opposite RVE boundaries, Γ is the external boundary of RVE,

(ii) linear displacement boundary conditions:

$$(2.4) \qquad u_j|_\Gamma = \varepsilon_{ij} x_i \rightarrow \langle \varepsilon_{ij} \rangle = \varepsilon_{ij},$$

(iii) uniform traction boundary conditions:

$$(2.5) \qquad t_j|_\Gamma = \sigma_{ij} n_i \rightarrow \langle \sigma_{ij} \rangle = \sigma_{ij}.$$

The averaged value of micro-stresses can be presented in terms of boundary reaction forces as:

$$(2.6) \qquad \langle \sigma_{ij} \rangle = \frac{1}{|V|} \int_V (\sigma_{ij}) \, dV = \frac{1}{|V|} \int_\Gamma (t_i \cdot x_j) \, d\Gamma = \frac{1}{|V|} \sum_{k=1}^n f_{ik} \cdot y_{jk},$$

where f_{in} is a reaction force on i-th direction of the n-th boundary node, y_{jn} represents the location in the j-th direction of the n-th boundary node.

In the case of the homogenisation procedure for materials in which the stress/strain relationship is linear, there is no need to analyse the RVE for each point of macrostructure, as there is an analytical model that represents the material properties at the macroscopic scale. To obtain equivalent properties, described by a 4$^{\text{th}}$ order material tensor, a number of analyses of RVE with specific boundary conditions have to be done. The number of analyses depends on the anisotropy type [34]. In the case of orthotropic material, 6 tests should be performed with unitary strain conditions (for each strain tensor component). An orthotropic material can be described by 9 independent stiffness coefficients, representing the stress/strain relationship, which can be expressed in the Voigt notation as:

$$(2.7) \qquad \begin{bmatrix} \sigma_{11} \\ \sigma_{22} \\ \sigma_{33} \\ \sigma_{23} \\ \sigma_{13} \\ \sigma_{12} \end{bmatrix} = \begin{bmatrix} C_{11} & C_{12} & C_{13} & 0 & 0 & 0 \\ & C_{22} & C_{23} & 0 & 0 & 0 \\ & & C_{33} & 0 & 0 & 0 \\ & & & C_{44} & 0 & 0 \\ & sym & & & C_{55} & 0 \\ & & & & & C_{66} \end{bmatrix} \begin{bmatrix} \varepsilon_{11} \\ \varepsilon_{22} \\ \varepsilon_{33} \\ 2\varepsilon_{23} \\ 2\varepsilon_{13} \\ 2\varepsilon_{12} \end{bmatrix},$$

where σ_{ij} and ε_{ij} are stress and strain tensor components, respectively, while C_{ij} are stiffness tensor components.

Computational homogenisation of non-linear materials involves the determination of a non-linear macro stress-strain relation. The process requires the solution of non-linear BVP in the micro-scale. The loading is applied incrementally. Each increase in loading causes change in the effective material constants [26]. Homogenisation results can be either effective tangent stiffness coefficients or the stress-strain relation. One can use experimental or numerical tests on non-homogeneous materials to develop the stress-strain relation, e.g. [35]. The present work uses a metamodel based on computational experiments and artificial neural network for the non-linear material.

3. Granular computations

The computational homogenisation methods presented in the previous Section can be enhanced to solve homogenisation problems with uncertain input data, e.g. by introducing granular computing methods.

Granular computing is a computing paradigm related to the processing of collections of complex units of information called grains or granules [36]. If the parameters of a system cannot be determined precisely, they can be treated as uncertain and modelled as grains of information [37]. Information grains are an element of abstraction found essentially everywhere, which is related to the human, intuitive – way of thinking, providing a link between the analogue real world and its digital representation in computing systems. Humans communicate with the outside world by building up and processing grains of information. The process of their creation is called information granulation. It can be granular in a spatial sense (spatial granulation) as well as in a temporal sense (temporal granulation). Information granules can be grouped according to similarity, coherence, indistinguishability, functional or geometric proximity criteria [38].

Each problem can be treated at various levels of granularity. Choosing the appropriate granularity allows relevant information to be made visible, and or details considered irrelevant to be omitted. Reducing grain size results in the inclusion of more detailed information, leading to higher computational costs [39]. In mechanical systems, granularity models related to uncertainties arising from both design and manufacturing processes are significant, and the analysis of uncertain data is crucial for the safety of the product [40]. The most commonly used granularity models for uncertainty include rough sets, interval numbers, fuzzy numbers and random variables.

Granular calculations can be introduced into the numerical homogenisation procedure. The uncertainties that can be used as model parameters can be related to geometry, material properties, loads, or boundary conditions. As a result of the analysis, a range of estimated quantities can be obtained. In the present

study, fuzzy numbers and interval numbers are considered uncertainty models. To reduce the problems with the application of classical interval arithmetic operations, directed interval arithmetic is applied.

3.1. Fuzzy numbers

According to [41], a fuzzy set is a class of objects with a continuous membership degree. If $\mathbb{X}$ is a nonempty set, a fuzzy set $\tilde{A}$ in X is characterized by its membership function $\mu_{\tilde{A}}(x)$ such as $\mu_{\tilde{A}} : \mathbb{X} \to [0, 1]$. Consequently, $\tilde{A}$ is fully determined by a set of pairs:

$$(3.1) \qquad \tilde{A} = \{(x, \mu_{\tilde{A}}(x)); \ x \in \mathbb{X}\}.$$

A fuzzy set defined in a real vector space which is normal (the maximum value of its membership function is equal to one), convex, and its membership function is piecewise continuous, is called a fuzzy number $\tilde{a}$ [42]. An extension principle allows us to apply the arithmetic operations performed on traditional sets to fuzzy numbers [43]. Unfortunately, the application of fuzzy arithmetic to solving systems of fuzzy equations is complicated as there are no fuzzy operations opposite to addition and reverse to multiplication.

To simplify fuzzy arithmetic operations, specific types of fuzzy numbers can be used, such as triangular or trapezoidal fuzzy numbers. A triangular fuzzy number can be represented as an ordered triple $\tilde{a} = (a^-, a_0, a^+)$. Triangular fuzzy numbers can be effectively applied to describe uncertain parameters with a known value and an estimation error, e.g. determined by an experiment. The use of triangular fuzzy numbers allows the simplification of basic arithmetic operations on fuzzy numbers [44]. An efficient method to avoid complex arithmetic operations on fuzzy numbers is to decompose the fuzzy number into a set
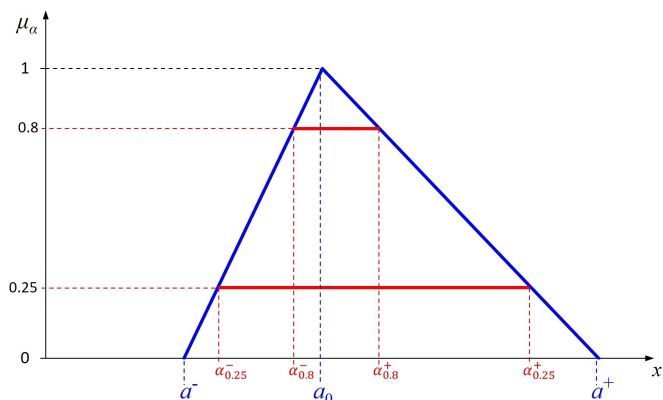

FIG. 1. Triangular fuzzy number and sample α-cuts ($\alpha = 0.25$, $\alpha = 0.8$).

of α-cuts. The α-cut of a fuzzy set $\tilde{A}$ in the space $\mathbb{X}$ is a non-fuzzy set for the values of the membership function are not less than α, for each $\alpha \in [0,1]$. The α-cut of triangular fuzzy number $\tilde{a}$ is a set of closed intervals:

$$(3.2) \qquad \forall \alpha \in [0,1] \quad \tilde{a}_\alpha = [(a_0 - a^-)\alpha + a^-, (a_0 - a^+)\alpha + a^+].$$

Any fuzzy set can be described as the sum of all its α-cuts. A triangular fuzzy set with exemplary α-cuts is presented in Fig. 1. The operations on fuzzy numbers described by α-cuts can be performed using interval number arithmetic, as presented in the next section.

3.2. Interval numbers and interval arithmetic

In issues where only a finite range of uncertain parameter values is known, interval numbers enable the representation of uncertainty. The interval representation of a single number is defined as [45]:

$$(3.3) \qquad \bar{a} = [a^-, a^+] = \{a \in \bar{a} : a^- \leq a \leq a^+\},$$

where a^- and $a^+ \in \mathbb{R}$ are left and right ends of the interval $\bar{a}$, respectively.

In contrast to fuzzy numbers, for interval numbers only two values of the membership function are possible: 1 if the number belongs to an interval, or 0 if the number does not belong to it. The interval is called degenerate if $a^- = a^+$.

The classical version of interval arithmetic is based on extended arithmetic for real numbers. Basic operations in classical interval arithmetic are addition, subtraction, multiplication, division, multiplication by scalar, and inverse of an interval [46]. The main disadvantage of classical interval arithmetic is the lack of additive and multiplicative inverses [47]. As a result, the interval widening occurs when solving interval systems of equations, e.g. by means of an interval Gaussian algorithm described further. The widening of an interval is a result of a series of calculations necessary to obtain a final solution. This effect can be significantly reduced by using the directed interval arithmetic. A directed interval number $\bar{a}$ is an ordered pair of real numbers:

$$(3.4) \qquad \bar{a} = [a^-, a^+] = \{a \in \mathbb{D}\},$$

where $\mathbb{D}$ is a set composed of all possible (proper and improper) directed interval numbers with real ends: $a^-, a^+ \in \mathbb{R}$ [48].

Depending on the position of the ends of the intervals, the directed interval numbers can be divided into proper (if $a^- < a^+$) and improper (if $a^- \geq a^+$), so $\mathbb{D} = \mathbb{P} \cup \mathbb{I}$, where $\mathbb{P}$ is a set of all proper interval numbers, $\mathbb{I}$ is a set of all improper interval numbers.

Directed interval arithmetic includes basic operations in the form of addition, subtraction, multiplication, and division. Moreover, directed interval arithmetic allows one to define new operators [49]:

$$(3.5) \qquad \forall \bar{a} \in \mathbb{D} \quad -_{\mathbb{D}} \bar{a} = [-a^-, a^+],$$

and:

$$(3.6) \qquad \forall \bar{a} \in \mathbb{D} \setminus \mathbb{Z} \quad 1/_{\mathbb{D}} \bar{a} = \left[\frac{1}{a^-}, \frac{-1}{a^+} \right],$$

where: $\mathbb{Z} = \mathbb{Z}_{\mathbb{P}} \cup \mathbb{Z}_{\mathbb{I}}$ contains all (proper and improper) directed intervals with element 0:

$$(3.7) \qquad \begin{aligned} \mathbb{Z}_{\mathbb{P}} &= \{ \bar{a} \in \mathbb{P} : a^- \le 0 \le a^+ \}, \\ \mathbb{Z}_{\mathbb{I}} &= \{ \bar{a} \in \mathbb{I} : a^+ \le 0 \le a^- \}. \end{aligned}$$

On the basis of them, two directed operations are introduced, namely:
– directed subtraction:

$$(3.8) \qquad \forall \bar{a}, \bar{b} \in \mathbb{D} \quad \bar{a} -_{\mathrm{D}} \bar{b} = [a^- - b^-, a^+ - b^+],$$

– directed division:

$$(3.9) \qquad \bar{a}/_{\mathbb{D}} \bar{b} = \begin{cases} [a^{-\sigma(\bar{b})}/b^{-\sigma(\bar{a})}, a^{\sigma(\bar{b})}/b^{\sigma(\bar{a})}], & \bar{a}, \bar{b} \in \mathbb{D} \backslash \mathbb{Z}, \\ [a^{-\sigma(\bar{b})}/b^{\sigma(\bar{b})}, a^{\sigma(\bar{b})}/b^{\sigma(b)}], & \bar{a} \in \mathbb{Z}, \bar{b} \in \mathbb{D} \backslash \mathbb{Z}, \end{cases}$$

where the 'sign' functional σ is defined as:

$$(3.10) \qquad \forall \bar{a} \in \mathbb{D} \backslash \mathbb{Z} \quad \sigma(\bar{a}) = \begin{cases} + & \text{if } a^- \ge 0, \\ - & \text{if } a^+ \le 0, \\ + & \text{if } a^- = a^+ = 0. \end{cases}$$

The σ and $-\sigma$ used in the superscript indicate whether the left or right end of an interval appears in the formula (e.g. a^+ or a^-), depending on whether it is a proper or improper number. In particular, $-\sigma$ changes specific end from left to right or right to left, respectively.

As a result, the operations $\bar{a} -_{\mathbb{D}} \bar{a} = \bar{0}$ and $\bar{a}/_{\mathbb{D}} \bar{a} = \bar{1}$ can be obtained. They allow for the efficient solution of interval equations with a significant reduction in interval widening [50]. A comparison of the results obtained using the classical and directed interval arithmetic shows much narrower outcome intervals for the latter approach [51].

4. Response surfaces

Granular computations described in the previous section involve multiple evaluations of the function under consideration. When the FEM is applied to evaluate such a function, the calculations may be time- and memory-consuming due to preprocessing, solution of the system of equations and postprocessing. One can reduce the cost by, e.g. using response surfaces.

Response surfaces (RS) belong to model reduction methods [52]. They allow one to build a metamodel representing the output parameters on the basis of an analysis of the results for the parameterised model. RS represents an approximate parametric model of the original system created from a precalculated set of models with various input parameter values. The accuracy of the metamodel is significantly dependent on the number of data points, the shape of the exact response function that is approximated, and the volume of the design space in which the model is built. RSs enable highly non-linear model behaviour to be modelled, without complex mathematical operations on the system matrices.

To minimise the computational effort required to prepare the data for the generation of RS, the design of experiment (DoE) should be used [53]. The DoE and the applied RS type strongly depend on the behaviour of the expected output parameters [54]. If the output parameter behaviour can be characterised as monotonic and close to linear, Central Composite Design (CCD) methods may be applied. The CCD methods are a five-level fractional factorial design, which is suitable for generating quadratic response models. The main idea is to distribute the samples in the centres as well as in the extreme and diagonal values of the input parameters design space, which can be typically represented by $[-\gamma, -1, 0, +1, +\gamma]$ values. The $[-1, 1]$ values are related to the limits of the
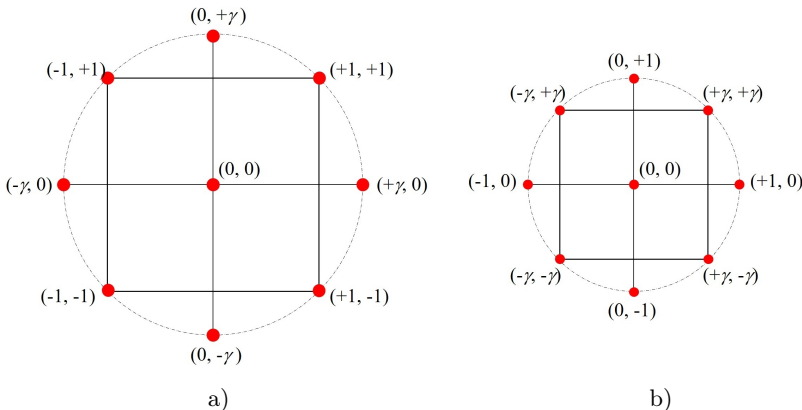

Fig. 2. Examples of CCD for two input parameters: a) CCC, b) CCI.

normalised input parameter range, while the $[-\gamma, +\gamma]$ values depend on the type of the CCD design, as presented in Fig. 2 for circumscribed (CCC) and inscribed (CCI) variants of CCD.

In cases where the behaviour of the output parameters is highly non-linear and multi-modal, DoE based on a regular discretisation of the design space, e.g. Optimal Space Filling, is recommended [55].

In the present paper, two different types of RS have been used, namely the 2nd order polynomial method and Artificial Neural Networks.

4.1. Second order polynomial method

The 2nd order polynomial method utilises an extended quadratic form to represent the relationship between input and output parameters. This method allows the response to be modelled for unimodal or monotonic functions and is thus ideally suited for solving optimisation problems, due to the generation of smooth functions with a single extremum. The quadratic model for a function y of n variables is of the form [56]:

$$(4.1) \qquad y = \beta_0 + \sum_{i=1}^{n} \beta_i x_i + \sum_{i=1}^{n} \sum_{j=i}^{n} \beta_{ij} x_i x_j,$$

where $\mathbf{B} = [\beta_0 \; \beta_1 \; \beta_2 \; \ldots \; \beta_n \; \beta_{11} \ldots \; \beta_{1n} \; \beta_{22} \ldots \; \beta_{2n} \; \ldots \; \beta_{nn}]^T$ denotes a vector of the polynomial coefficients while $\mathbf{x}$ is a vector of input parameters.

After selecting the M design points using the DoE ($M \geq$ size($\mathbf{B}$), where size($\mathbf{B}$) denotes a number of elements in $\mathbf{B}$), an RS metamodel is constructed using the least squares method. The unknown polynomial coefficients $\boldsymbol{\beta}$ are calculated taking into account the sum of squares error SSE between the exact results of the analysis y_i and the polynomial approximation y'_i:

$$(4.2) \qquad SSE = \sum_{i=1}^{M} (y_i - y'_i)^2 = \sum_{i=1}^{M} \varepsilon_i^2,$$

where $\varepsilon_i = y_i - y'_i$ is called the residual.

The residuals can be represented as follows:

$$(4.3) \qquad \boldsymbol{\varepsilon} = \mathbf{y} - \mathbf{XB},$$

where $\mathbf{X}$ is the samples input values matrix, e.g. in the following form (the coefficients are obtained in an order corresponding to inserted input parameters data):

(4.4) $\quad$ $\mathbf{X} =$

$$
\begin{bmatrix}
1 & x_{11} & x_{21} & & x_{n1} & x_{11}x_{21} & x_{11}x_{31} & & x_{(n-1)1}x_{n1} & x_{11}^2 & x_{21}^2 & & x_{n1}^2 \\
1 & x_{12} & x_{22} & \cdots & x_{n2} & x_{12}x_{22} & x_{12}x_{32} & \cdots & x_{(n-1)2}x_{n2} & x_{12}^2 & x_{22}^2 & \cdots & x_{n2}^2 \\
1 & x_{13} & x_{23} & & x_{n3} & x_{13}x_{23} & x_{13}x_{33} & & x_{(n-1)3}x_{n3} & x_{13}^2 & x_{23}^2 & & x_{n3}^2 \\
& & & & & \vdots & & & & & & \\
1 & x_{1m} & x_{2m} & & x_{nm} & x_{1m}x_{2m} & x_{1m}x_{3m} & & x_{(n-1)m}x_{nm} & x_{1m}^2 & x_{2m}^2 & & x_{nm}^2
\end{bmatrix},
$$

and x_{nm} denotes an n-th input parameter value for the m-th sample of the *SSE*. The *SSE* then takes the form:

(4.5) $$ SSE = \boldsymbol{\varepsilon}^{\mathrm{T}}\boldsymbol{\varepsilon} = (\mathbf{y} - \mathbf{X}\mathbf{B})^{\mathrm{T}}(\mathbf{y} - \mathbf{X}\mathbf{B}). $$

As a result of differentiating Eq. (4.5) and equating it to zero, the vector of polynomial coefficients $\mathbf{B}$ can be calculated as:

(4.6) $$ \mathbf{B} = (\mathbf{X}^{\mathrm{T}}\mathbf{X})^{-1}\mathbf{X}^{\mathrm{T}}\mathbf{y}. $$

4.2. Artificial Neural Networks as response surfaces

One of the possible applications of artificial neural networks (ANNs) is the creation of response surfaces. ANNs are inspired by the functioning of nerve cells (neurons) present in the human brain and nervous system [57]. The artificial neuron consists of multiple inputs with the corresponding weighting coefficient and a single output. A feed-forward ANN consists of many neurons arranged in layers: input, output, and (optionally) one or more hidden layers [58]. The output signal for an i-th neuron of the ANN is calculated as:

(4.7) $$ y_i = \omega\Big(\sum_{j=0}^{N} w_{ij}x_j\Big) = \omega\Big(\sum_{j=1}^{N} w_{ij}x_j + B\Big), $$

where y_i is an output value the i-th neuron, ω denotes an activation function, w_{ij} is the weighting coefficient for j-th input value, x_j states a j-th input value of the i-th neuron, $B = w_{i0}x_0$ is the neuron bias.

The activation function is related to the type of problem to be solved. Within the framework of this paper, a sigmoid activation function is adopted:

(4.8) $$ \omega(x) = \frac{1}{1 + e^{-\psi x}}, $$

where ψ is a coefficient related to the slope of the function.

The use of ANN as RS allows the modelling of complex data relationships involving multimodal, highly non-linear, and discontinuous functions. To prepare

the ANN for the description of parameter relationships, network learning has to be carried out. The aim of learning is to modify the weighting factors in such a way as to obtain the required ANN response for the given input values. In the present paper, the Levenberg–Marquardt algorithm implemented in the MATLAB software is used [59].

4.3. Response surface quality metrics

To verify the quality of the created RS, quality metrics should be used to determine the precision of the values of the output parameters mapped [60]. The metrics applied in the paper are:

- The coefficient of determination R^2:

$$(4.9) \qquad R^2 = 1 - \frac{\sum_{i=1}^{N}(y_i - y_i')^2}{\sum_{i=1}^{N}(y_i - \bar{y})^2},$$

  where $\bar{y}$ denotes the mean value of the output samples vector, N is a number of samples. The R^2 values belong to the range from 0 to 1; $R^2 = 1$ represents the perfect mapping of the input samples values.

- The standard error of the estimate σ_{est}:

$$(4.10) \qquad \sigma_{est} = \sqrt{\frac{\sum_{i=1}^{N}(y_i - y_i')^2}{N}} = \sqrt{MSE},$$

  where MSE denotes the mean squared error. The $\sigma_{est} = 0$ indicates a perfect match between the input samples and output values of RS.

- The predicted residual error sum of squares $PRESS$:

$$(4.11) \qquad PRESS = \sum_{i=1}^{N}(y_i^{ver} - y_i')^2,$$

  where $\mathbf{y}^{ver}$ is a vector of verification samples.

5. Granular Computational Homogenisation

The aim of the homogenisation is to obtain possible ranges of equivalent macroscopic linear material properties that depend on assumed uncertainties. In this paper, the Granular Computational Homogenisation (GCH) concept is proposed to solve uncertain homogenisation problems. GCH is based on the representation of the microstructure of the material, the response surfaces of different forms, the interval numbers, and the directed interval arithmetic [61]. Fuzzy numbers decomposed into α-cuts allow for the application of more detailed

input data information than only input ranges. Such an approach leads to a safer design of components made of inhomogeneous materials than in the case of typical calculations without assumed uncertainties. The general concept of GCH is presented in Fig. 3. The commercial finite element method software (ANSYS) is used to solve boundary value problems on the micro scale.
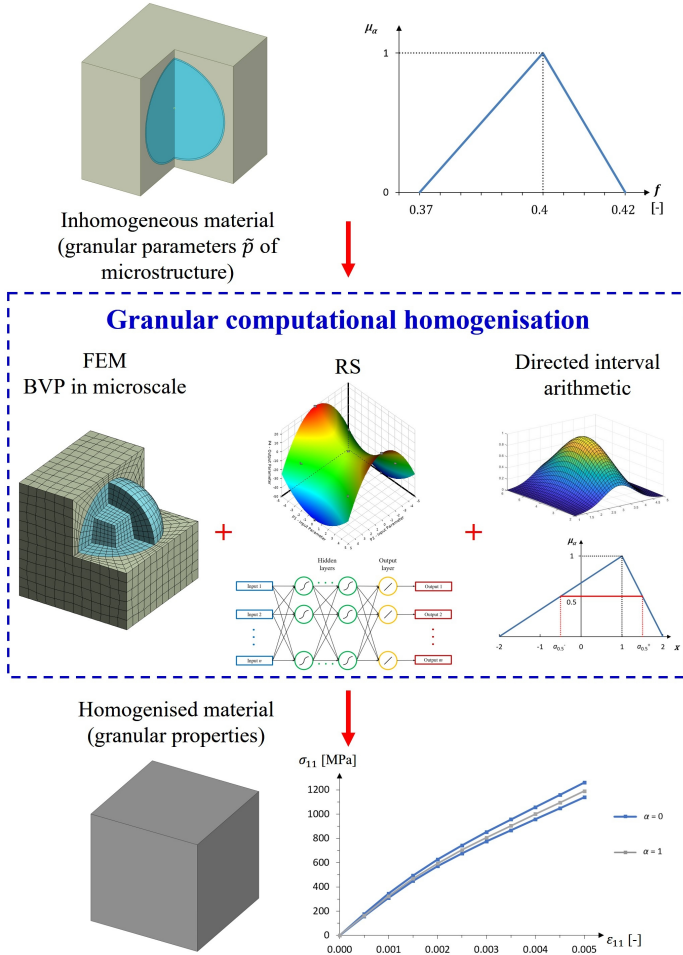

Fig. 3. Concept of Granular Computational Homogenisation.

The first step in the granular homogenisation scheme (Fig. 4) is to prepare a geometrical model of the structure (RVE) based on the microstructure of the material. The model is then transferred to the ANSYS software. Based on the geometry and assumed material properties, including constitutive relationships, non-linearities, and the type of uncertainty, a numerical model of the microstructure is created. Information on the uncertainty of the data allows the selection
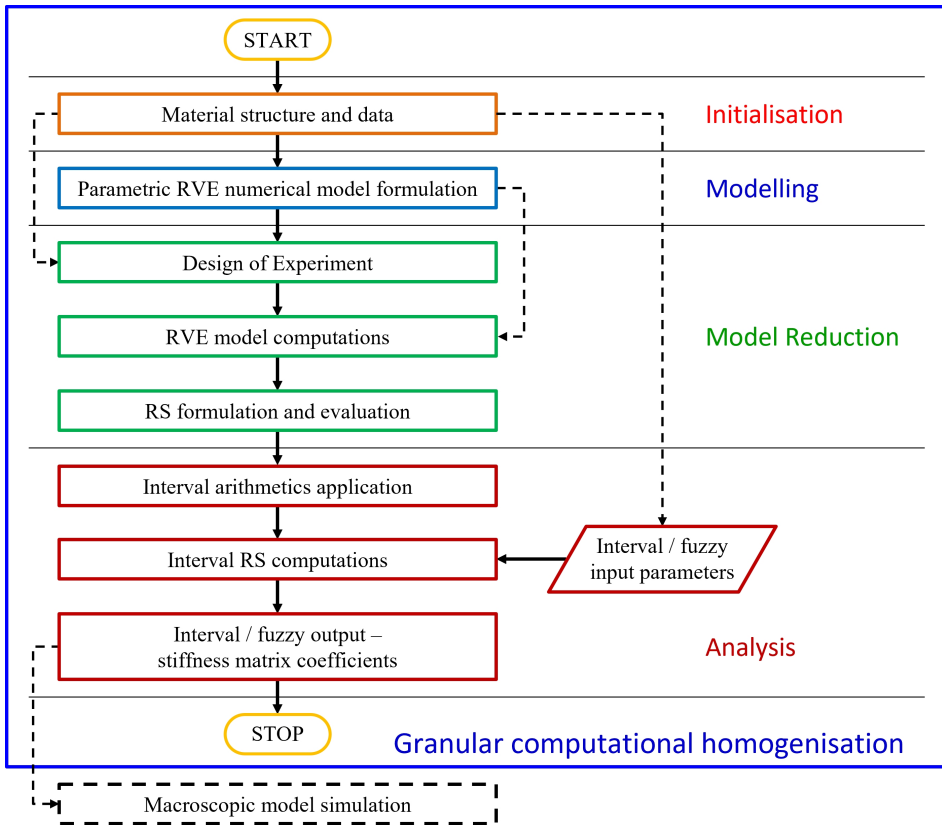
FIG. 4. Granular Computational Homogenisation scheme.

of the uncertainty modelling method (interval/fuzzy approach). The number of input parameters influences the number of necessary sample calculations in the DoE phase.

In the next step, the RS is generated on the input/output data. The RS is constructed from RVEs calculated using classical numerical homogenisation. Once the RS has been generated, the metamodel is represented as a set of algebraic expressions that map the input parameters to the output parameters. The equations of the metamodel are rewritten by introducing the directed interval arithmetic, which results in the interval RS. The interval calculations result in the values of the interval output parameters, representing the stiffness matrix coefficients with assumed uncertainty type (interval numbers or α-cuts of the fuzzy numbers). The uncertain stiffness matrix coefficients for linear materials and stress/strain curves for non-linear materials are calculated as output parameters.

6. Numerical results

In the present section, the application of the GCH to numerical homogenisation of inhomogeneous materials with uncertainties is presented. All computations were performed usinga notebook workstation with an Intel Core i7-8750H processor (6 cores with $2.2\,\mathrm{GHz}$ clock speed) and $32\,\mathrm{GB}$ of RAM.

6.1. Fibre-reinforced linear material

A fibre-reinforced composite made of an epoxy resin matrix with a uniform and unidirectional distribution of carbon fibres is considered. The properties of the homogeneous components of the composite are assumed to be experimentally determined, and some of them are treated as uncertain. To obtain possible ranges of equivalent, macroscopic material properties, the computational homogenisation based on material microstructure representation, 2nd order polynomial RS, and fuzzy representation of uncertainties are employed.

Uncertain parameters are represented as triangular fuzzy numbers represented by three values each (a^-, a_0, a^+), where the value of a_0 can differ from the mean value of the left and right ends of the fuzzy number (a^-, a^+). Such an approach allows the asymmetry of the fuzzy number to be modelled. Each fuzzy number is represented by twelve α-cuts. The a_0 values have been taken from [62].

The properties of the isotropic matrix material are as follows:
– the uncertain matrix Young's modulus: $\tilde{E}_m = (4.5, 4.8, 5.1)\,\mathrm{GPa}$;
– the certain matrix Poisson's ratio: $\nu_m = 0.3$.

The properties of the transversally isotropic fibre material are the following:
– uncertain Young's modulus in the fibre longitudinal x_1 direction: $\tilde{E}_{f1} = (245, 250, 265)\,\mathrm{GPa}$;
– uncertain Young's modulus in the fibre transverse x_2 direction $\tilde{E}_{f2} = (21.5, 22.4, 23.3)\,\mathrm{GPa}$;
– uncertain Kirchhoff's modulus in the $x_1 x_2$ plane

$$\tilde{G}_{f12} = (20.7, 22.1, 22.9)\,\mathrm{GPa};$$

– certain Poisson's ratios $\nu_{f12} = 0.3$ and $\nu_{f23} = 0.35$.
It is assumed that the volume fraction of reinforcement is also uncertain: $\tilde{f} = (0.37, 0.4, 0.42)$.

The microstructure of the material is represented by an RVE of dimensions $30 \times 30 \times 30\,\mu\mathrm{m}$ containing 9 uniformly distributed parallel fibres. The range of fibre radii, resulting from the assumed volume fraction, is $3.432 \div 3.657\,\mu\mathrm{m}$ (Fig. 5a) [63]. The periodic boundary conditions are imposed on the RVE. The RVE is discretised into 29 484 high-quality hexahedral elements with quadratic shape functions (Hex20), resulting in 373 593 DoFs (Fig. 5b).
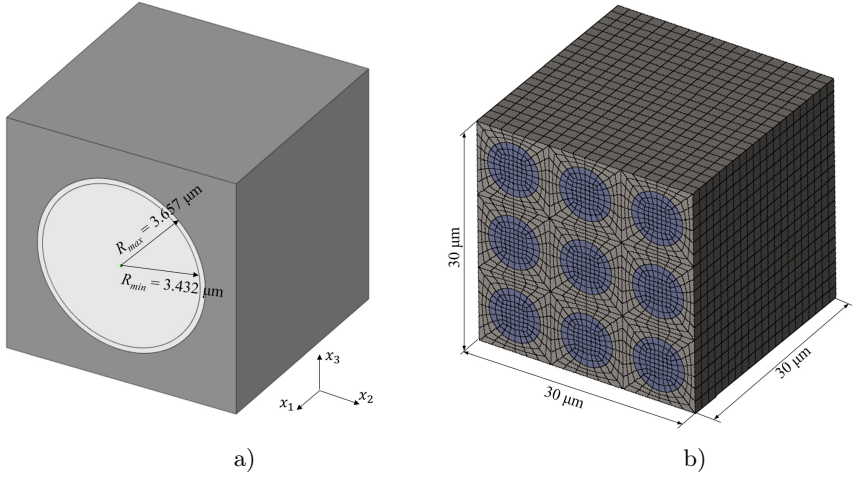
Fig. 5. The RVE model of the fibre-reinforced composite material:
a) unit cell geometry, b) FEM mesh.

The relative difference between the exact and discretised volume of reinforcement depends on the volume fraction, while the maximum value obtained is equal to $6.515 \times 10^{-4}\%$. As the volume difference associated with the change in volume fraction is 4 orders of magnitude greater than the error of the geometric approximation, the second one can be assumed to be negligible.

The assumption of a uniform fibre distribution results in an orthotropic material with two equivalent perpendicular directions (x_2 and x_3). Consequently, the number of independent stiffness coefficients is equal to six: C_{11}, $C_{12} = C_{13}$, $C_{22} = C_{33}$, C_{23}, C_{44}, $C_{55} = C_{66}$ (see Eq. (2.7)). DoE in the form of the CCF variant of the Central Composite Design method was performed to create RS in terms of a 2nd order polynomial, resulting in 43 sets of necessary input parameters. Then, the output parameters were calculated using periodic boundary conditions. After calculating the design points, the 21 coefficients of the 2nd order polynomial RS were calculated as:

$$(6.1) \qquad C^{RS}(i,j) = \beta_0(i,j) + \sum_{k=1}^{5} \beta_k(i,j)p_k + \sum_{k,l} \beta_{kl}(i,j)p_k p_l,$$

where p_i is the i-th parameter value ($p_1 = E_m$, $p_2 = E_{f1}$, $p_3 = E_{f2}$, $p_4 = G_{f12}$, $p_5 = f$) and the pair $kl \in \{11, 12, 13, 14, 15, 22, 23, 24, 25, 33, 34, 35, 44, 45, 55\}$.

The computed RS coefficients and quality metric values are collected in Table 1. To calculate the *PRESS* metric values, additional 15 sets of random combinations of parameters were used. The quality metrics indicate an excellent match between the samples and RS.

Table 1. RS coefficients and quality metrics for fibre-reinforced composite material.

Coefficient	$C^{RS}(1,1)$	$C^{RS}(1,2)$	$C^{RS}(2,2)$	$C^{RS}(2,3)$	$C^{RS}(4,4)$	$C^{RS}(5,5)$
$\beta_0(i,j)$	$3.792{\times}10^{-1}$	$6.595{\times}10^{-1}$	$1.952{\times}10^{0}$	$3.441{\times}10^{-1}$	$5.326{\times}10^{-1}$	$1.614{\times}10^{0}$
$\beta_1(i,j)$	$1.512{\times}10^{0}$	$7.760{\times}10^{-1}$	$1.605{\times}10^{0}$	$7.453{\times}10^{-1}$	$3.718{\times}10^{-1}$	$2.762{\times}10^{-1}$
$\beta_2(i,j)$	$4.373{\times}10^{-5}$	$7.339{\times}10^{-5}$	$1.239{\times}10^{-4}$	$1.224{\times}10^{-4}$	$8.258{\times}10^{-6}$	$2.130{\times}10^{-5}$
$\beta_3(i,j)$	$-1.899{\times}10^{-2}$	$-3.169{\times}10^{-2}$	$-9.493{\times}10^{-2}$	$-1.069{\times}10^{-2}$	$-1.224{\times}10^{-2}$	$2.310{\times}10^{-4}$
$\beta_4(i,j)$	$1.987{\times}10^{-5}$	$3.755{\times}10^{-5}$	$6.670{\times}10^{-5}$	$7.194{\times}10^{-5}$	$5.546{\times}10^{-5}$	$-2.360{\times}10^{-2}$
$\beta_5(i,j)$	$-1.925{\times}10^{0}$	$-3.348{\times}10^{0}$	$-9.909{\times}10^{0}$	$-1.748{\times}10^{0}$	$-2.706{\times}10^{0}$	$-8.208{\times}10^{0}$
$\beta_{11}(i,j)$	$-2.077{\times}10^{-2}$	$-3.313{\times}10^{-2}$	$-7.662{\times}10^{-2}$	$-2.907{\times}10^{-2}$	$-1.485{\times}10^{-2}$	$-1.691{\times}10^{-2}$
$\beta_{12}(i,j)$	$-1.951{\times}10^{-5}$	$-3.113{\times}10^{-5}$	$-4.966{\times}10^{-5}$	$-4.964{\times}10^{-5}$	$-9.129{\times}10^{-9}$	$1.440{\times}10^{-11}$
$\beta_{13}(i,j)$	$9.130{\times}10^{-3}$	$1.456{\times}10^{-2}$	$3.342{\times}10^{-2}$	$1.305{\times}10^{-2}$	$6.378{\times}10^{-3}$	$4.455{\times}10^{-10}$
$\beta_{14}(i,j)$	$-7.162{\times}10^{-9}$	$1.362{\times}10^{-9}$	$2.499{\times}10^{-10}$	$-3.219{\times}10^{-10}$	$2.179{\times}10^{-10}$	$7.481{\times}10^{-3}$
$\beta_{15}(i,j)$	$-1.014{\times}10^{0}$	$5.185{\times}10^{-2}$	$2.938{\times}10^{-1}$	$1.040{\times}10^{-1}$	$2.697{\times}10^{-1}$	$9.716{\times}10^{-1}$
$\beta_{22}(i,j)$	$2.474{\times}10^{-7}$	$3.934{\times}10^{-7}$	$6.264{\times}10^{-7}$	$6.232{\times}10^{-7}$	$-1.507{\times}10^{-8}$	$-4.176{\times}10^{-8}$
$\beta_{23}(i,j)$	$-1.609{\times}10^{-6}$	$-2.567{\times}10^{-6}$	$-4.115{\times}10^{-6}$	$-4.075{\times}10^{-6}$	$-6.055{\times}10^{-9}$	$-1.451{\times}10^{-11}$
$\beta_{24}(i,j)$	$2.156{\times}10^{-9}$	$2.907{\times}10^{-11}$	$9.335{\times}10^{-12}$	$-2.482{\times}10^{-11}$	$-3.917{\times}10^{-12}$	$-8.530{\times}10^{-12}$
$\beta_{25}(i,j)$	$9.997{\times}10^{-1}$	$-4.299{\times}10^{-4}$	$-7.010{\times}10^{-4}$	$-6.943{\times}10^{-4}$	$-1.225{\times}10^{-6}$	$6.812{\times}10^{-11}$
$\beta_{33}(i,j)$	$-9.695{\times}10^{-4}$	$-1.547{\times}10^{-3}$	$-3.559{\times}10^{-3}$	$-1.375{\times}10^{-3}$	$-6.835{\times}10^{-4}$	$-5.155{\times}10^{-6}$
$\beta_{34}(i,j)$	$1.187{\times}10^{-9}$	$2.211{\times}10^{-10}$	$3.022{\times}10^{-10}$	$8.679{\times}10^{-12}$	$4.086{\times}10^{-11}$	$-2.396{\times}10^{-11}$
$\beta_{35}(i,j)$	$1.245{\times}10^{-1}$	$2.021{\times}10^{-1}$	$5.383{\times}10^{-1}$	$1.181{\times}10^{-1}$	$7.863{\times}10^{-2}$	$-3.121{\times}10^{-9}$
$\beta_{44}(i,j)$	$-4.747{\times}10^{-7}$	$-8.617{\times}10^{-7}$	$-1.530{\times}10^{-6}$	$-1.650{\times}10^{-6}$	$-1.272{\times}10^{-6}$	$-8.223{\times}10^{-4}$
$\beta_{45}(i,j)$	$1.427{\times}10^{-6}$	$2.946{\times}10^{-8}$	$5.611{\times}10^{-9}$	$-5.215{\times}10^{-9}$	$-3.108{\times}10^{-9}$	$1.142{\times}10^{-1}$
$\beta_{55}(i,j)$	$2.425{\times}10^{0}$	$4.220{\times}10^{0}$	$1.250{\times}10^{1}$	$2.195{\times}10^{0}$	$3.416{\times}10^{0}$	$1.037{\times}10^{1}$
R^2	0.9999	0.9999	0.9999	0.9999	0.9999	0.9999
σ_{est}	$1.835{\times}10^{-4}$	$2.993{\times}10^{-4}$	$7.164{\times}10^{-4}$	$2.597{\times}10^{-4}$	$1.438{\times}10^{-4}$	$2.715{\times}10^{-4}$
$PRESS$	$2.285{\times}10^{-7}$	$6.054{\times}10^{-7}$	$3.577{\times}10^{-6}$	$4.184{\times}10^{-7}$	$1.350{\times}10^{-7}$	$3.362{\times}10^{-7}$

To reconstruct the output fuzzy numbers, calculations of the ranges of the output parameters are performed for all α-cuts of each input parameter. Verification of the ranges of determined stiffness coefficients is performed by comparing the fuzzy output numbers for 0 and 1 of the α-cut with the semi-empirical results of the Halpin–Tsai theory (with a modified reinforcement factor for E_2 calculations) [64]. The results of the comparison are summarised in Table 2.

The computation time for each design point for the four homogenisation tests was approximately 60 s; the total computation time for all design points was ∼45 min. The total time to create RS and evaluate the interval numbers was less than 1 s. Although the application of the presented methodology leads to a longer computation time than a single analysis of all combinations for deterministic systems (due to the larger number of RVE samples required), the

TABLE 2. Effective elastic constants of the fibre-reinforced material.

Material stiffness coefficients [GPa]		Halpin–Tsai solution	RS + Fuzzy numbers	Relative difference [%]
$\tilde{C}_{11}$	min ($\alpha = 0$)	96.355	96.331	0.024
	middle ($\alpha = 1$)	106.006	105.980	0.024
	max ($\alpha = 0$)	117.620	117.593	0.023
$\tilde{C}_{12}$	min ($\alpha = 0$)	4.498	4.480	0.385
	middle ($\alpha = 1$)	4.915	4.896	0.378
	max ($\alpha = 0$)	5.299	5.280	0.366
$\tilde{C}_{22}$	min ($\alpha = 0$)	9.879	9.914	−0.354
	middle ($\alpha = 1$)	10.872	10.915	−0.397
	max ($\alpha = 0$)	11.772	11.825	−0.453
$\tilde{C}_{23}$	min ($\alpha = 0$)	4.224	4.198	0.622
	middle ($\alpha = 1$)	4.584	4.553	0.678
	max ($\alpha = 0$)	4.924	4.886	0.766
$\tilde{C}_{44}$	min ($\alpha = 0$)	2.633	2.486	5.617
	middle ($\alpha = 1$)	2.908	2.732	6.060
	max ($\alpha = 0$)	3.158	2.959	6.292
$\tilde{C}_{55}$	min ($\alpha = 0$)	3.241	3.252	−0.326
	middle ($\alpha = 1$)	3.660	3.678	−0.474
	max ($\alpha = 0$)	4.029	4.053	−0.592

generation of RS enables a fast metamodel application for optimisation and identification problems. In this case, the time spent on a single RS generation and its computation is much shorter than the total time related to the need to analyse numerous deterministic RVEs for each set of optimisation parameters.

A careful analysis of the resulting fuzzy numbers presented in 6.2 shows that they are no longer triangular due to the slight distortion, especially for values of the membership function close to 1. This is due to the non-linear relationship between input and output parameters.

The comparison of the result ranges with the semi-empirical model shows very high agreement between the generated RS and the numerical model for almost all stiffness coefficients (the absolute relative difference is less than 0.68%). The maximum absolute relative difference of 6.29% was obtained for the coefficient $\tilde{C}_{44}$ and is related to the smaller values obtained by the numerical model with periodic boundary conditions than with the Halpin–Tsai equations. This discrepancy may be related to the simplifications adopted in analytical solutions and has also been reported by other authors (e.g. [65]).
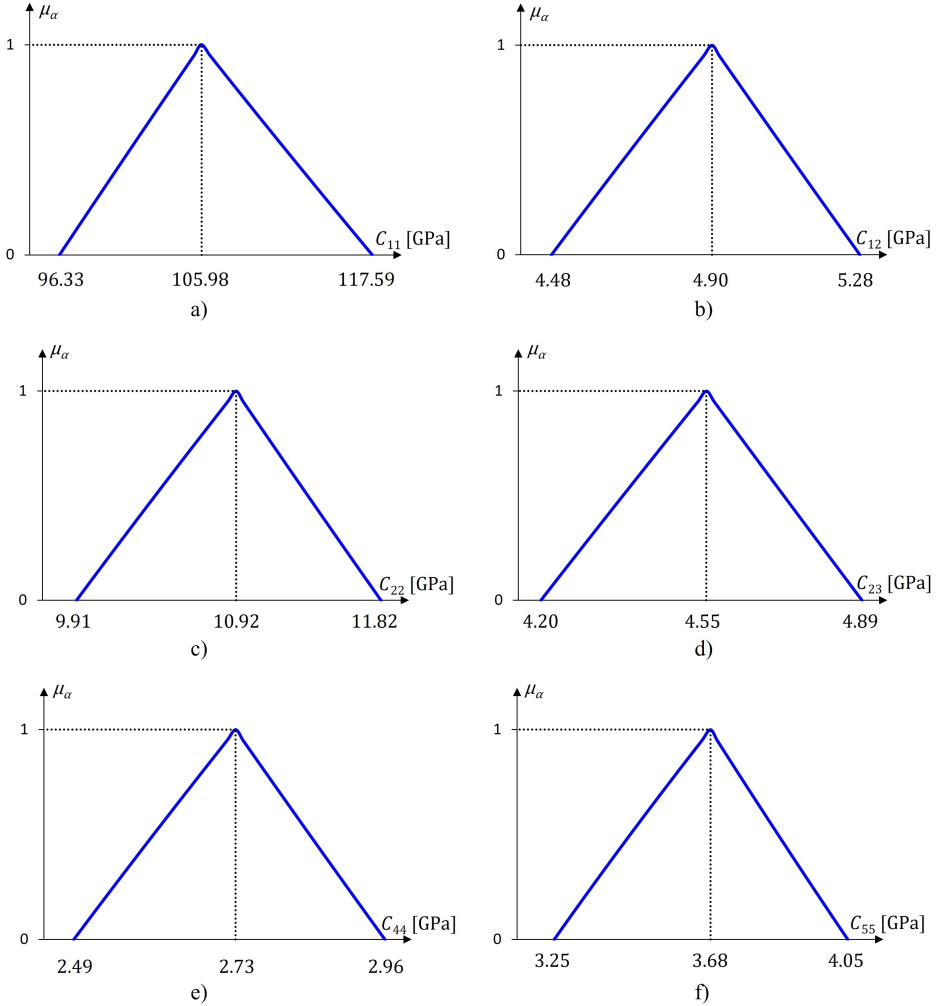
Fig. 6. The fuzzy representation of effective elastic constants for the fibre-reinforced composite material: a) $\tilde{C}_{11}$, b) $\tilde{C}_{12}$, c) $\tilde{C}_{22}$, d) $\tilde{C}_{23}$, e) $\tilde{C}_{44}$, f) $\tilde{C}_{55}$.

6.2. Particle-reinforced non-linear material

A composite material for surface coatings made of a non-linear nickel alloy (NiCrBSi) matrix with uniformly distributed linear tungsten carbide inclusions is considered. The bilinear isotropic properties [66] are assumed for the matrix material. Such coatings with thicknesses up to 2 mm are used due to their wear properties [67]. As the thickness of the coating is usually relatively small compared to the thickness of the object to be coated, the shear stiffness of the coating can be neglected. As a consequence, the important effective properties of the composite are related to the response to the normal strain [68].

The properties of the homogeneous components of the composite are assumed to be experimentally determined, and some of them are treated as uncertain. To obtain possible ranges of equivalent, macroscopic non-linear material properties, the computational homogenisation based on material microstructure representation, neural network RS and fuzzy representation of uncertainties are used.

The uncertain parameters represented as triangular fuzzy numbers are as follows:

- matrix Young's modulus $\tilde{E}_m = (157.95, 162, 170.1)\,\text{GPa}$;
- matrix yield stress $\tilde{R}_{em} = (318.5, 325, 331.5)\,\text{MPa}$;
- reinforcement Young's modulus $\tilde{E}_r = (666.4, 680, 700.4)\,\text{GPa}$;
- the reinforcement volume fraction $\tilde{f} = (0.304, 0.32, 0.332)$.

The a_0 values of triangular fuzzy numbers have been taken from [69]. The remaining, certain properties are:

- matrix Poisson's ratio $\nu_m = 0.3$;
- the matrix tangent modulus $E_{Tm} = 3.25\,\text{GPa}$;
- reinforcement Poisson's ratio $\nu_r = 0.315$.

The microstructure of the composite material is represented by a $2 \times 2 \times 2\,\text{mm}$ periodic unit cell (RVE) containing a single centrally located spherical inclusion (Fig. 7a). The R_{min} and R_{max} inclusion radii values are the result of the assumed volume fraction range.

Since only the non-linear normal strain response is relevant for determining the behaviour of a relatively thin shell, a single non-linear normal strain uniform test is sufficient. The unit cell geometry is discretised into 8,640 hexahedral elements with quadratic shape functions (Hex20), resulting in 103,773 DoFs (Fig. 7b). The influence of the discretisation on the geometrical uncertainty has

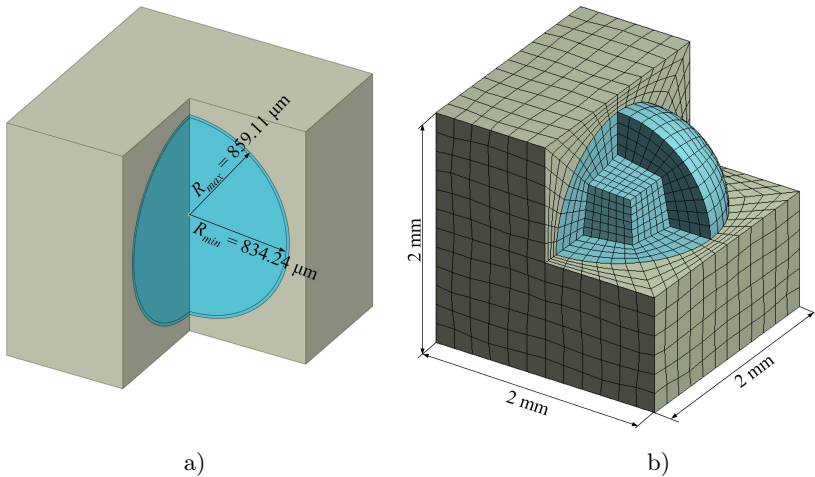a)   b)

Fig. 7. Unit cell model for particle-reinforced composite material:
a) geometry, b) finite element mesh.

been checked. The maximum value of the relative difference between the theoretical and discretised geometry volume of reinforcement is equal to $4.498 \times 10^{-4}\%$ while the volume difference associated with a change in the volume fraction is four orders of magnitude greater. As a result, the effect of discretisation on geometric uncertainty can be neglected.

The Optimal Space Filling algorithm has been used as the DoE to create 50 design points that discretise the space of the input parameters. The stress response for 10 increasing strain load values from the range $\varepsilon_{11} = \langle 0, 0.005 \rangle$ has been stored during the analysis. To obtain a metamodel capable of representing the non-linear stress response, strain load values have been used as an additional input parameter. A 2-layer 5-5-2 ANN has been created using the MATLAB neural network toolbox (Fig. 8). A sigmoidal activation function with the ψ coefficient equal to 2 was applied for hidden layer neurons while a linear activation function was adopted for both output layer neurons.
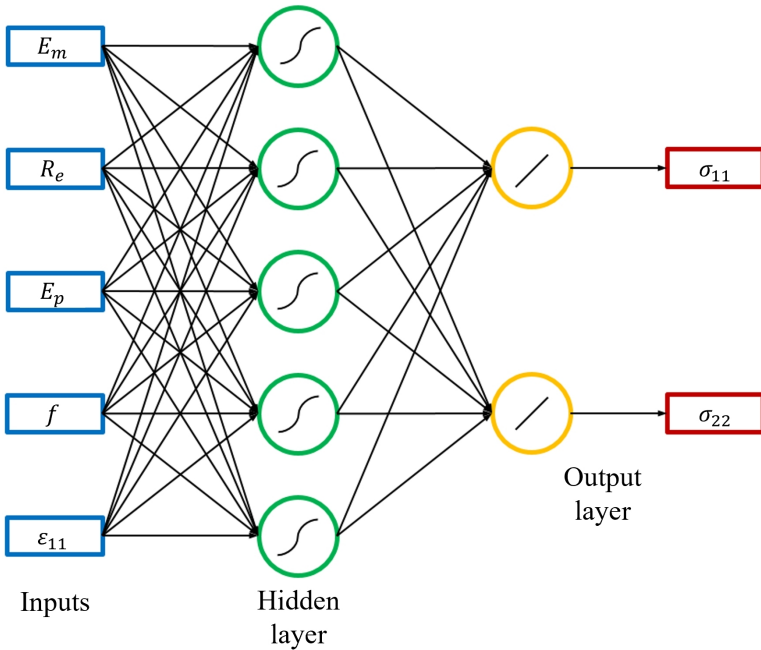

Fig. 8. The neural network architecture for particle-reinforced non-linear material.

70% of the set of calculated parameters were used to obtain the neuron coefficients, while the remaining 30% were used for the ANN testing. The training algorithm converged after 509 iterations, obtaining a mean squared error of $\text{MSE} = 4.191\,\text{MPa}^2$, which is relatively small compared to the calculated values of the stiffness matrix coefficients. The coefficient of determination $R^2 = 0.999$,

thus the neural network describes the non-linear behaviour of the material with sufficient accuracy.

The computation time for each design point for homogenisation tests was approximately 15 min; the total computation time for all design points was ~12.5 h. The creation and training time of the ANN was approximately 30 s, while the evaluation time of the interval numbers was less than 1 s.

To analyse the effects of uncertainties, the trained neural network was transformed using Eq. (4.7) into algebraic expressions that describe the values of the output parameters. These equations were modified by introducing interval arithmetic. To apply fuzzy calculations, fuzzy numbers were introduced for the first four input parameters using their α-cuts, obtaining a set of interval equations for all α-cut levels analysed. The strain input parameter was used as an additional variable for the calculation of fuzzy numbers. The input fuzzy numbers were discretised into 15 α-cuts each to reconstruct the output fuzzy number with an unknown shape of the membership function. The results of the calculations in the form of fuzzy macroscopic stresses σ_{ij} for strain values $\varepsilon_{11} = 0.0025$ and $\varepsilon_{11} = 0.005$ are shown in Fig. 9.
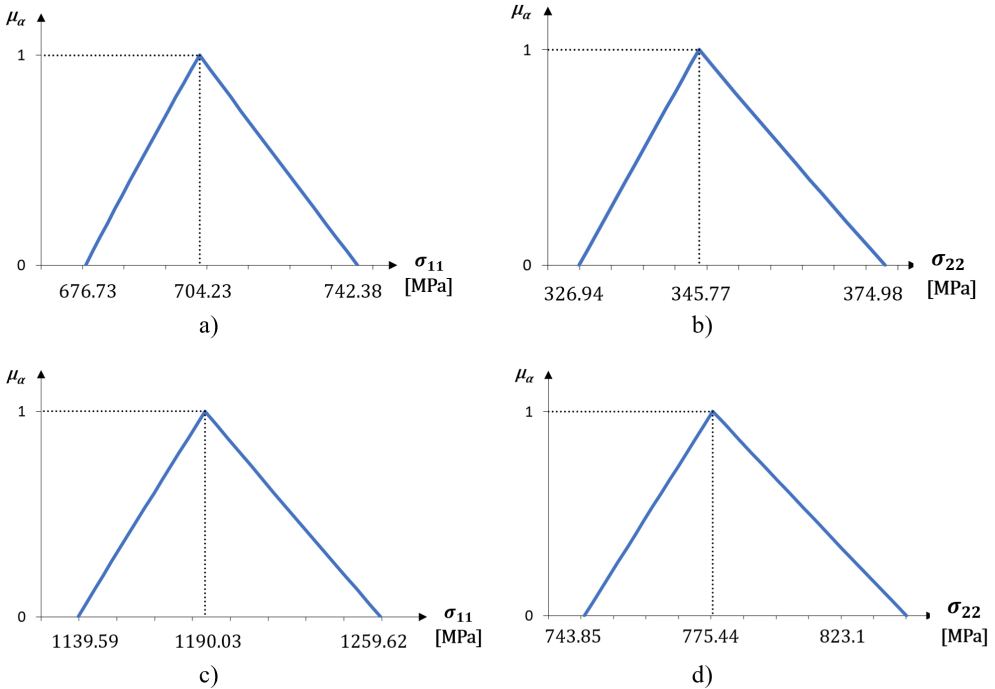

FIG. 9. Fuzzy σ_{ij} macroscopic stress representation for specified ε_{11} values for particle reinforced material: a) σ_{11} for $\varepsilon_{11} = 0.0025$, b) σ_{22} for $\varepsilon_{11} = 0.0025$, c) σ_{11} for $\varepsilon_{11} = 0.005$, d) σ_{22} for $\varepsilon_{11} = 0.005$.

A two-dimensional projection of fuzzy σ_{ij}–ε_{11} relationship is shown in Fig. 10. The membership functions in red correspond to the σ_{ij} coefficients for $\varepsilon_{11} = 0.0025$ and $\varepsilon_{11} = 0.005$.

To verify the RVE numerical model and the results of the non-linear calculations, ranges of effective elastic properties were calculated using the Cohen theory [70] by calculating the sets of input parameters related to the extreme values of the ranges of the parameters. The results in the form of stress-strain relationship are presented in Fig. 10 with dotted lines. The comparison shows good agreement with the first steps of the analysis of the non-linear model. The calculated stress-strain relations are non-linear functions. The nonlinearity is caused by the plastic yield of the matrix, in which the von Mises stresses exceed the yield stress.
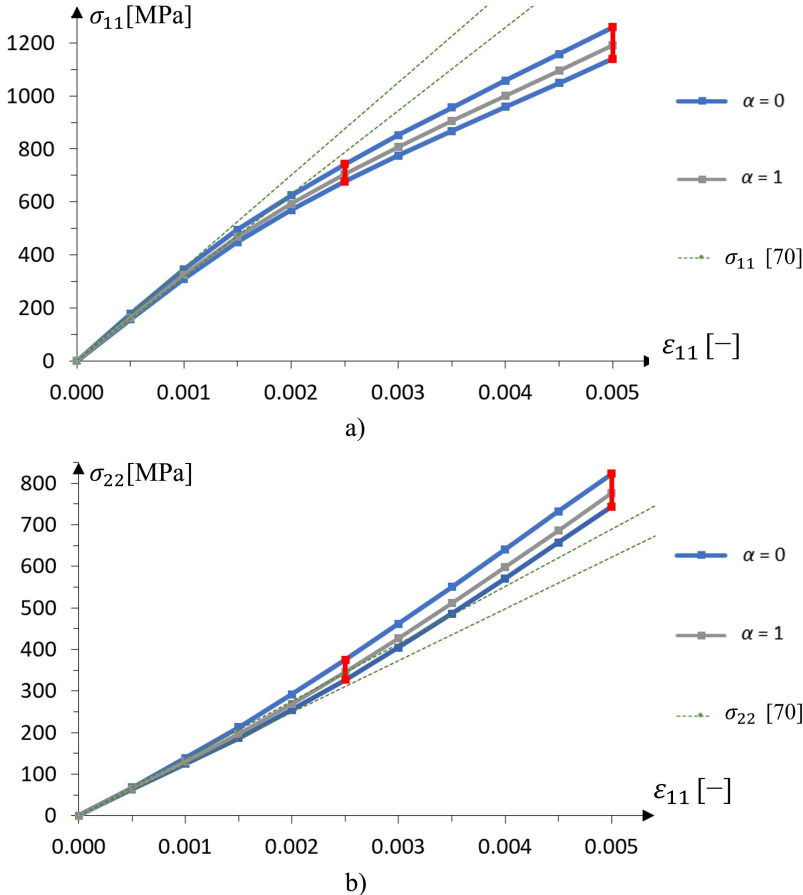

Fig. 10. Two-dimensional projection of fuzzy σ_{ij}–ε_{11} relationship for particle-reinforced material: a) for σ_{11} and b) for σ_{22}.

The two-dimensional projection of the fuzzy relationship σ_{ij}–ε_{11} shows the non-linear behaviour of the RVE model during longitudinal strain loading. As the material matrix is described by the bilinear hardening rule, the tangent stiffness C_{11} decreases with increasing load, while the tangent stiffness C_{12} increases. It can also be seen in Fig. 10 that the output parameters are asymmetric, which is due to the asymmetry of the input parameters. Furthermore, the width of the fuzzy number described by α-cut for $\alpha = 0$ increases with strain load, indicating that the uncertainty of the material behaviour also increases with higher strain values.

7. Conclusions

This paper presents the granular computational homogenisation, which is a novel approach to the computational homogenisation of heterogeneous materials with uncertain parameters. Two types of information granularities in the form of interval numbers and fuzzy numbers are used. Converting fuzzy numbers to sets of α-cuts allows the application of interval arithmetic in both cases. Linear and non-linear material behaviours are considered. The model order reduction in the form of response surfaces (2$^{\text{nd}}$ order polynomials and Artificial Neural Networks) have been proposed to speed up computation, which is particularly important for a non-linear material behaviour where the incremental analysis is performed.

Numerical examples show the efficiency and high accuracy of the proposed approach. The most time-consuming operation is the calculation of DoE samples, while the amount of time required for the other operations is considerably lower. The created RS can be reused to solve other granulometric homogenisation problems, assuming the same microstructure of the material. The use of interval arithmetic eliminates the need to calculate different samples to find the minimum and maximum values of the stiffness coefficients. The accuracy of the proposed method is confirmed by comparing it with traditional computational homogenisation and analytical methods.

The presented approach uses the directed interval arithmetic, which minimises the effect of interval widening. This feature may be advantageous in future applications, e.g. identification of imprecise microstructure parameters based on measured or desired properties of the structure on the macro scale. The application of conventional interval arithmetic would cause unwanted interval widening in such cases. Another approach to efficiently solve such problems may be to include the sensitivity analysis for parameter intervals [71].

The proposed approach can be used successfully to solve actual scientific and industrial problems with uncertainties. The GCH can also be embedded in commercial software, making the method applicable to a wide range of users.

Conflict of interest

Acknowledgements

References

1. S.W. Tsai, H.T. Hahn, *Introduction to Composite Materials*, Technomic Publishing Company, Lancaster, 1980.

2. S.G. Advani, E.M. Sozer, *Process Modeling in Composites Manufacturing*, Marcel Dekker, New York, 2003.

3. J. Ptaszny, P. Fedeliński, G. Dziatkiewicz, *Boundary element method modelling of nanocomposites*, International Journal for Multiscale Computational Engineering, **12**, 1, 33–43, 2014.

4. J. Ptaszny, M. Hatłas, *Evaluation of the FMBEM efficiency in the analysis of porous structures*, Engineering Computations, **35**, 2, 843–866, 2018.

5. J. Ptaszny, *A fast multipole BEM with higher-order elements for 3-D composite materials*, Computers & Mathematics with Applications, **82**, 15, 148–160, 2021.

6. T.S. Mesogitis, A.A. Skordos, A.C. Long, *Uncertainty in the manufacturing of fibrous thermosetting composites: a review*, Composites Part A: Applied Science and Manufacturing, **57**, 67–75, 2014.

7. M. Kamiński, *Homogenization of particulate and fibrous composites with some non-Gaussian material uncertainties*, Composite Structures, **210**, 778–786, 2019.

8. M.A. Bessa, R. Bostanabad, Z. Liu, A. Hu, D.W. Apley, C. Brinson, W. Chen, W.K. Liu, *A framework for data-driven analysis of materials under uncertainty: countering the curse of dimensionality*, Computer Methods in Applied Mechanics and Engineering, **320**, 633–667, 2017.

9. R. Bostanabad, B. Liang, J. Gao, W.K. Liu, J. Cao, D. Zeng, X. Su, H. Xu, Y. Li, W. Chen, *Uncertainty quantification in multiscale simulation of woven fiber composites*, Computer Methods in Applied Mechanics and Engineering, **38**, 506–532, 2018.

10. B. Möller, M. Beer, *Fuzzy Randomness: Uncertainty in Civil Engineering and Computational Mechanics*, Springer, Berlin, Heidelberg, 2004.

11. M. Kamiński, M. Kleiber, *Perturbation based stochastic finite element method for homogenization of the two-phase elastic composites*, Computers and Structures, **78**, 811–826, 2000.

12. W. Beluch, T. Burczyński, *Two-scale identification of composites' material constants by means of computational intelligence methods*, Archives of Civil and Mechanical Engineering, **14**, 636–646, 2014.

13. S. Naskar, T. Mukhopadhyay, S. Sriramula, *Spatially varying fuzzy multi-scale uncertainty propagation in unidirectional fibre reinforced composites*, Composite Structures, **209**, 940–967, 2019.

14. W. Beluch, M. Hatłas, *Numerical homogenization of inhomogeneous media with imprecise parameters*, Computer Methods in Mechanics, AIP Conference Proceedings, **1922**, 1–7, 2017.

15. A.I. Khuri, J.A. Cornell, *Response Surfaces: Designs and Analyses*, 2nd ed., CRC Press, Boca Raton, 1996.

16. M.S. Kothari, K.G. Vegad, K.A. Shah, A. Aly Hassan, *An artificial neural network combined with response surface methodology approach for modelling and optimization of the electro-coagulation for cationic dye*, Heliyon, **8**, 1, e08749, 2022.

17. E.R. Hansen, *A generalized interval arithmetic*, [in:] K. Nickel [ed.], *Interval Mathematics*, Lecture Notes in Computer Science, **29**, 7–18, 1975.

18. B. Sendov, *Some Topics of Segment Analysis*, Interval Mathematics, K. Nickiel [ed.], Academic Press, pp. 203–222, New York, 1980.

19. S.M. Markov, *On directed interval arithmetic and its applications*, Journal of Universal Computer Science, **1**, 514–526, 1995.

20. T.-W. Hou, *Microstructural Design of Fiber Composites*, Cambridge University Press, Cambridge, 1992.

21. J. Ptaszny, P. Fedeliński, *Numerical homogenization of polymer/clay nanocomposites by the boundary element method*, Archives of Mechanics, **63**, 517–532, 2011.

22. J. Ptaszny, *Accuracy of the fast multipole boundary element method with quadratic elements in the analysis of 3D porous structures*, Computational Mechanics, **56**, 3, 477–490, 2015.

23. T. Czyż, G. Dziatkiewicz, P. Fedeliński, R. Górski, J. Ptaszny, *Advanced Computer Modelling in Micromechanics*, Silesian University of Technology Press, Gliwice, 2013.

24. M. Hatłas, W. Beluch, *Multiscale global identification of porous structures*, Computer Methods in Mechanics, AIP Conference Proceedings, **1922**, 1–7, 2017.

25. W. Beluch, A. Długosz, *Multiobjective and multiscale optimization of composite materials by means of evolutionary computations*, Journal of Theoretical and Applied Mechanics, **52**, 2, 397–409, 2016.

26. D. Gross, T. Seelig, *Fracture Mechanics, with an Introduction to Micromechanics*, Springer, Berlin, Heidelberg, 2006.

27. T. Lewiński, J. Telega, *Plates, laminates and Shells: Asymptotic Analysis and Homogenization*, World Scientific, 2000.

28. A. Belkhabbaz, R. Brenner, N. Rupin, B. Brigitte, J. Fonseca, *Prediction of the overall behavior of a 3D microstructure of austenitic steel by using FFT numerical scheme*, Procedia Engineering, **10**, 1883–1888, 2011.

29. O. Pierard, C. Friebel, I. Doghri, *Mean-field homogenization of multi-phase thermoelastic composites: a general framework and its validation*, Composites Science and Technology, **64**, 1587–1603, 2004.

30. T. ZOHDI, P. WRIGGERS, *An Introduction to Computational Micromechanics*, Springer, Berlin, Heidelberg, 2005.

31. M. GEERS, V. KOUZNETSOVA, K. MATOUS, J. YVONNET, *Homogenization methods and multiscale modeling: Nonlinear problems*, Encyclopedia of Computational Mechanics, 2nd ed., pp. 1–34, 2017.

32. R. HILL, *Elastic properties of reinforced solids: some theoretical principles*, Journal of the Mechanics and Physics of Solids, **11**, 357–372, 1963.

33. M.G.D. GEERS, V. KOUZNETSOVA, T. MASSART, I. ÖZDEMIR, E.W.C. COENEN, W.A.M. BREKELMANS, R.H.J. PEERLINGS, *Computational homogenization of structures and materials*, Proceedings of the 9th Neuvième Colloque National en Calcul des Structures, Giens, France, pp. 17–28, 2009.

34. L. BOS, P. GIBSON, M. KOTCHETOV, M.A. SLAWINSKI, *Classes of anisotropic media: a tutorial*, Studia Geophisica et Geodaetica, **48**, 265–287, 2004.

35. S. GATEA, T. JWAD, F. CHEN, H. OU, *Micromechanical modeling of the deformation and damage behavior of al6092/sic particle metal matrix composites*, Journal of Materials Engineering and Performance, 2023, doi: 10.1007/s11665-023-07907-4.

36. L.A. ZADEH, *Fuzzy sets and information granularity*, [in:] N. Gupta, R. Ragade, R, Yager [eds.], *Advances in Fuzzy Set Theory and Applications*, pp. 3–18, Amsterdam, North Holland, 1979.

37. A.A. RAMLI, J. WATADA, W. PEDRYCZ, *Information granules problem: an efficient solution of real-time fuzzy regression analysis*, [in:] W. Pedrycz, S.M. Chen [eds.], *Information Granularity, Big Data, and Computational Intelligence. Studies in Big Data*, **8**, Springer, Cham, 2015.

38. A. BARGIELA, W. PEDRYCZ, *Toward a theory of granular computing for human-centred information processing*, IEEE Transactions on Fuzzy Systems, **16**, 2, 320–330, 2008.

39. J.T. YAO, *A ten-year review of granular computing*, Proceeding of 2007 IEEE International Conference on Granular Computing, Silicon Valley, USA, pp. 734–739, 2007.

40. B.M. AYYUB, *Uncertainty Modeling and Analysis in Civil Engineering*, CRC Press, Boca Raton, 1997.

41. L.A. ZADEH, *Fuzzy sets*, Information and Control, **8**, 338–353, 1965.

42. D. DUBOIS, H. PRADE, *Operations on fuzzy numbers*, International Journal of Systems Science, **9**, 613–626, 1978.

43. M. HANSS, *Applied Fuzzy Arithmetic*, Springer, Berlin, 2005.

44. M.L. GUERRA, L. STEFANINI, *Approximate fuzzy arithmetic operations using monotonic interpolations*, Fuzzy Set and Systems, **150**, 5–33, 2005.

45. P.R. HALMOS, *Naive Set Theory*, Springer, New York, 1974.

46. L. JAULIN, M. KIEFFER, O. DIDRIT, E. WATER, *Applied Interval Analysis*, Springer, London, 2001.

47. B. HAYES, *A lucid interval*, American Scientist, **91**, 6, 484–488, 2003.

48. S.M. MARKOV, *On direct interval arithmetic and its applications*, Journal of Universal Computer Science, **1**, 7, 514–526, 1995.

49. E.D. Popova, *Multiplication distributivity of proper and improper intervals*, Reliable Computing, **7**, 129–140, 2001.

50. S.M. Markov, *Extended interval arithmetic involving infinite intervals*, Mathematica Baltanica, **6**, 269–304, 1992.

51. A. Piasecka-Belkhayat, *Interval boundary element method for imprecisely defined unsteady heat transfer problems* [in Polish], Publishing House of Silesian University of Technology, Monographs, **321**, Gliwice, 2011.

52. P.R. Nelson, M. Coffin, K.A.F. Copeland, *Response surface methods*, P.R. Nelson, M. Coffin, A.F.K. Copeland [eds.], *Introductory Statistics for Engineering Experimentation*, pp. 395–423, Academic Press, Cambridge, 2003.

53. D. Montgomery, *Design and Analysis of Experiments*, John Wiley & Sons, New York, 2012.

54. L.W. Friedman, *The Simulation Metamodeling*, Springer, Boston, 1996.

55. L. Prozato, W. Müller, *Design of computer experiments: space filling and beyond*, Statistics and Computing, **22**, 681–701, 2012.

56. J.P.C. Kleijnen, *Response Surface Methodology*, [in:] M. Fu [ed.], *Handbook of Simulation Optimization. International Series in Operations Research and Management Science*, **216**, Springer, New York, 2015.

57. L. Rutkowski, *Computational Intelligence: Methods and Techniques*, Springer, Berlin, 2008.

58. J. Hertz, R.G. Palmer, A.S. Krogh, *Introduction to the Theory of Neural Computation*, Perseus Books, New York, 1990.

59. M.T. Hagan, M. Menhaj, *Training feed-forwards networks with Marquardt algorithm*, IEEE Transactions on Neural Networks, **5**, 989–993, 1994.

60. *Ansys Inc.: Theory Reference*, Release 19.0 documentation for ANSYS, 2018.

61. M. Hatłas, *Modelling and Optimisation of Inhomogeneous Materials Using Granular Computations*, PhD Thesis, Gliwice, 2021.

62. J. German, *Basics of Fibre-reinforced Composite Mechanics*, Cracow University of Technology, Cracow, 1996 [in Polish].

63. G.G. Tibbetts, C.P. Beetz, *Mechanical properties of vapour-grown carbon fibres*, Journal of Physics D: Applied Physics, **20**, 3, 292–297, 1987.

64. E. Giner, A. Vercher, M. Marco, *Estimation of the reinforcement factor ξ for calculating E_2 with the Halpin-Tsai equations using the finite element method*, Composite Structures, **124**, 402–408, 2015.

65. Y. Fan, H. Wang, *A simple Python code for computing effective properties of 2D and 3D representative volume element under periodic boundary conditions*, Project: Reanalysis Assisted Global Optimization, Cornell University, 2017.

66. B. Chatterjee, P. Sahoo, *Effect of strain hardening on elastic-plastic contact of a deformable sphere against a rigid flat under full stick contact condition*, Advances in Tribology, **2012**, Article ID 472794, 8 pages, 2012.

67. D. DESCHUYTENEER, F. PETIT, M. GONON, F. CAMBIER, *Influence of large particle size – up to 1.2 mm – and morphology on wear resistance in NiCrBSi/WC laser cladded composite coatings*, Surface & Coatings Technology, **311**, 365–373, 2017.

68. L.I. TUSHINSKY, I. KOVENSKY, A. PLOKHOV, V. SINDEYEV, P. RESHEDKO, *Coated metal. Structure and properties of metal-coating compositions*, *Engineering Materials*, Springer, New York, 2002.

69. Z. HU, R. KARKI, *Prediction of mechanical properties of three-dimensional fabric composites reinforced by transversely isotropic carbon fibers*, Journal of Composite Materials, **49**, 1513–1524, 2015.

70. I. COHEN, *Simple algebraic approximations for the effective elastic moduli of cubic arrays of spheres*, Journal of the Mechanics and Physics of Solids, **52**, 2167–2183, 2004.

71. G. SHAO, J. SU, *Sensitivity and inverse analysis methods for parameter intervals,* Journal of Rock Mechanics and Geotechnical Engineering, **2**, 3, 274–280, 2010.